



Direct thermal enhancement dominates over emission-mediated pathways in heatwave-induced O₃ and SOA increases across China

Peng Wang^{1,2,3*}, Wenxuan Yu^{4,5}, Zhaolei Zhang⁴, Jianyan Lu^{1,6}, Shenxin Li⁷, Hongliang Zhang^{7,2,5*}

5 ¹Department of Atmospheric and Oceanic Sciences, Fudan University, Shanghai 200438, China.

²Institute of Eco-Chongming (IEC), Shanghai 202151, China.

³Shanghai Key Laboratory of Ocean-land-atmosphere Boundary Dynamics and Climate Change, Shanghai 200438, China.

⁴Department of Environmental Science & Engineering, Fudan University, Shanghai, 200438, China.

10 ⁵IRDR ICoE on Risk Interconnectivity and Governance on Weather/Climate Extremes Impact and Public Health, Fudan University, Shanghai 200438, China.

⁶Shanghai Frontiers Science Center of Atmosphere-Ocean Interaction, Shanghai 200438, China.

⁷School of Environment and Architecture, University of Shanghai for Science and Technology, Shanghai 200093, China

Correspondence to: Peng Wang (w_peng@fudan.edu.cn) and Hongliang Zhang (zhanghl@usst.edu.cn)

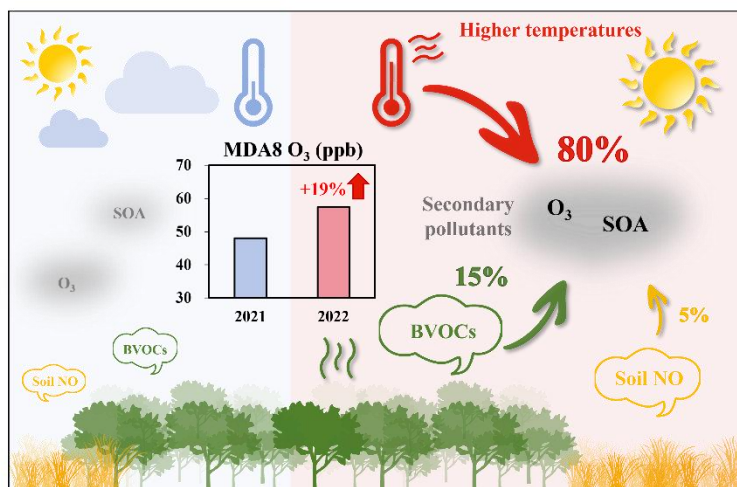
Abstract. Heatwaves are major drivers of ozone (O₃) and secondary organic aerosol (SOA) pollution. High temperatures
15 directly accelerate photochemical reaction rates and concurrently enhance emissions of biogenic volatile organic compounds (BVOCs) and soil nitric oxide (SNO). However, the individual contributions of these direct and emission-mediated pathways to pollution formation remain poorly constrained. This study explicitly quantifies the distinct roles of these two pathways during heatwave events in China. Results show that high temperatures drive over 80% of the O₃ and SOA increases nationally, primarily through favorable weather conditions and enhanced atmospheric oxidation capacity. The O₃-temperature dependence
20 is strongest in the Yangtze River Delta (0.66 ppb °C⁻¹) and Pearl River Delta (0.95 ppb °C⁻¹). Furthermore, high-temperature-induced BVOC emissions significantly exacerbate O₃ in VOC-limited regions like the North China Plain. These findings underscore the importance of climate mitigation by illustrating its critical role in alleviating temperature-driven secondary pollution.

25

30



35 Graphical abstract.



1 Introduction

The Chinese government has implemented stringent emission control policies since 2013, achieving substantial reductions in primary pollutants sulfur dioxide (SO₂) and nitrogen dioxide (NO₂) (Weng et al., 2023; Zheng et al., 2017; Zhang et al., 2019; Zhao et al., 2018). However, there were still heavy pollution events driven by secondary pollutants such as ozone (O₃) and secondary organic aerosol (SOA) (Shao et al., 2023; Wang et al., 2019; An et al., 2019; Wang et al., 2021b). In 2022, the observed O₃ concentration across 337 cities in China reached an average of 68 ppb, a 5.8% increase from 2021, with even higher levels in major city clusters. For instance, the Chengdu Plain experienced 17 consecutive days of O₃ pollution in August 2022 (Wang et al., 2024). Similarly, widespread severe haze events were also largely driven by secondary components like SOA (Zhang et al., 2024; Huang et al., 2014; Duan et al., 2020; Lin et al., 2024; Huang et al., 2020; Huang et al., 2021). These trends raise growing concern, as exposure to elevated surface O₃ and SOA poses serious threats to human respiratory health, crop yields and climate (Huang et al., 2018; Li et al., 2022; Hu and Guo, 2020; Li et al., 2020; Oh et al., 2023).

Secondary pollutant concentrations are directly or indirectly influenced by meteorological conditions, which affect their formation, transport, and removal processes (Mousavinezhad et al., 2021; Bai et al., 2022). Regarding direct effects, high temperatures could accelerate O₃ formation rates including those involving hydrogen oxide radicals (HO_x) (Eremenko et al., 2008; Filleul et al., 2006; Otero et al., 2016; Meng et al., 2023). Synoptic patterns, such as high-pressure systems and low wind speeds further exacerbate O₃ accumulation by suppressing vertical and horizontal diffusion (Liu and Wang, 2020). These impacts are even more pronounced in urban areas due to the urban heat island effect, which intensifies local warming (Oke, 1982; Conti et al., 2005; Luo and Lau, 2017; Sun et al., 2014). An et al. (2023) reported the slope between maximum daily 8-



55 hour average (MDA8) O₃ and daily maximum temperature (T_{max}) was 0.49 ppb °C⁻¹ steeper in urban areas than in rural areas, resulting in heightened O₃ pollution.

As for the indirect effects, rising temperatures enhance emissions of biogenic volatile organic compounds (BVOCs) and soil NO (SNO), key precursors that drive secondary pollutant production (Guenther et al., 2012; Chang et al., 2009; Seco et al., 2022; Huang et al., 2023; Li et al., 2024). Based on measurements and model simulations, Zhang et al. (2023) found that high
60 temperature drove an 18% yr⁻¹ isoprene increase at a suburban Hong Kong site, leading to a 0.44 ppb h⁻¹ yr⁻¹ O₃ elevation. Besides, modeling studies also reported a 20% increase in summertime biogenic SOA over North Europe under a 2.5°C temperature rise (Megaritis et al., 2013). Beyond BVOCs, Oikawa et al. (2015) proved a positive correlation between SNO and temperature, which in turn aggravated secondary pollution. Although the impact of high temperatures on air quality has been widely recognized, the relative contributions of direct effects versus indirect emission-mediated pathways (e.g., via
65 BVOCs and SNO) are still largely unknown.

This study quantifies the direct and indirect contributions of high temperatures to O₃ and SOA concentrations during the record-breaking 2022 summer heatwave in China, using coupled Weather Research and Forecasting (WRF) and Community Multiscale Air Quality (CMAQ) modeling. The year was defined by an unprecedented summer of extreme heat, which had its most severe impact across the Yangtze River Basin (YRB) (Lu et al., 2023). Results show that ~80% of the increases in O₃
70 and SOA are attributed to the direct impacts of high-temperature meteorology. These findings imply that effective mitigation of secondary pollution calls for integrated controls targeting both anthropogenic emissions and climate-driven warming.

2 Materials and Methods

2.1 Model Configuration

CMAQ version 5.4 with a modified SAPRC-11 photochemical mechanism was applied with a horizontal resolution of 36km
75 × 36km. The WRF version 4.2.2 was utilized to generate meteorology inputs, driven by initial and boundary conditions from National Centers for Environmental Prediction (NCEP) Final Reanalysis Data (FNL) with a high resolution of 0.25° × 0.25° (<https://rda.ucar.edu/datasets/ds083.2/>, last access: April 2024). Anthropogenic emissions were projected for 2021 and 2022 by adjusting the 2020 Multi-resolution Emission Inventory for China (MEIC) (<http://www.meicmodel.org>, last access: April 2024) with updated traffic and industrial emission data (Zheng et al., 2018) (**Supplementary Text S1**). Biogenic emissions
80 including BVOC and SNO were generated using the Model of Emissions of Gases and Aerosols from Nature (MEGAN) version 2.1 (Guenther et al., 2012). Overall, the simulation was acceptable for the analysis compared with the observations, and a detailed model validation is presented in **section 3.1**.

2.2 CMAQ O₃ Process Analysis

The process analysis tools embedded in the CMAQ model were applied in the following analysis. The Integrated Process Rate
85 (IPR) analysis was employed to quantify the contributions of key physical and chemical processes to O₃ formation and to



identify those most responsible for its increase (Byun, 1999). Seven processes in the IPR contributed to O₃ formation, including horizontal diffusion (HDIF), horizontal advection (HADV), vertical diffusion (VDIF), vertical advection (ZADV), gas-phase chemistry (CHEM), dry deposition (DDEP), and cloud processes (CLDS). In this study, the sum of VDIF and ZADV was classified as vertical transport (VTRA). The sum of HADV and HDIF was classified as horizontal transport (HTRA).

90 2.3 CMAQ Simulation Scenarios

The summer of 2022 was selected for its record-high temperatures, while the summer of 2021 served as a baseline representing typical meteorological conditions (Lu et al., 2023). Two base cases, BASE21 and BASE22, were configured with default settings for 2021 and 2022 (**Table 1**). To isolate the effects of meteorology, BVOC, and SNO emissions, three sensitivity cases MET22, BVOC22, and SNO22 were conducted. These cases simulated 2022 using 2021 meteorology (MET22), 2021 BVOC emissions (BVOC22), and 2021 SNO emissions (SNO22), respectively. These simulations allowed the total difference between the two years (BASE22 – BASE21, termed '22-21') to be partitioned into three components: (1) the direct meteorological effect (BASE22 – MET22, 'MET'), (2) the indirect effect from climate-driven BVOC emissions (BASE22 – BVOC22, 'BVOC'), and (3) the indirect effect from SNO emissions (BASE22 – SNO22, 'SNO'). Four major Chinese city clusters including the North China Plain (NCP), the Yangtze River Delta (YRD), the Chongqing-Sichuan region (CY), and the Pearl River Delta (PRD) were selected for detailed analysis (**Fig. 1a**).

Due to the nonlinearity of secondary pollution formation, summing these isolated contributions leaves a residual term when compared to the total difference. This term reflects the overlapping synergistic interactions between the high temperatures and elevated emissions concurrently present in the BASE22 scenario. To eliminate this arithmetic overlap and accurately quantify the relative importance of each driver, the percentage contributions presented in this study were normalized against the sum of absolute concentration changes from all separated scenarios.



Table 1. Simulation experiments design.

Cases	Case description
BASE21/BASE22	Meteorological and biogenic emission data from their respective years.
MET22	Simulation of 2022 by using 2021 meteorology
BVOC22	Simulation of 2022 by using 2021 BVOC emissions. Notes: Isoprene, terpenes, and sesquiterpenes were selected as they represent the dominant BVOC species (Guenther et al., 2012; Zhang et al., 2018).
SNO22	Simulation of 2022 by using 2021 SNO emissions

2.4 Response of Secondary Pollutants to Temperature and Emission Changes

To better quantify the response of secondary pollutants to meteorology and biogenic emissions, a best-fit slope method was applied. This method, previously applied to the O_3 - T_{max} relationship, was extended to SOA and biogenic emissions in this study (Wang et al., 2021a; Ma et al., 2019). Linear regression slope (k) and correlation coefficient (r) between secondary pollutants (MDA8 O_3 and SOA) and T_{max} , daily average temperature (T), BVOC and SNO emission rates were calculated, respectively. The equations are shown below (Su et al., 2012):

$$k = \frac{\sum_{i=1}^n x_i y_i - n \bar{x} \bar{y}}{\sum_{i=1}^n x_i^2 - n \bar{x}^2} \quad (1)$$

$$r = \frac{\sum_{i=1}^n (x_i - \bar{x})(y_i - \bar{y})}{\sqrt{\sum_{i=1}^n (x_i - \bar{x})^2} \sqrt{\sum_{i=1}^n (y_i - \bar{y})^2}} \quad (2)$$

where n is the total number of grids in the area, and x represents T_{max} , average temperature, BVOC and SNO emission rates, respectively. y denotes the concentrations of MDA8 O_3 and SOA. \bar{x} and \bar{y} are the average of x and y . The sensitivity of MDA8 O_3 is expressed in ppb $^{\circ}C^{-1}$ for temperature and ppb s mole $^{-1}$ for emissions. The sensitivity of SOA is expressed in μg m $^{-3}$ $^{\circ}C^{-1}$ for temperature and μg s (m $^{-3}$ mole $^{-1}$) for emissions. Because the calculated sensitivities to temperature and emissions possess incomparable units, these regression slopes were not normalized.

3 Results and Discussions

3.1 Model Evaluation

The simulation of meteorological conditions and pollutants was generally acceptable for the following analysis. Simulated 2-meter temperature (T2), relative humidity (RH), 10-meter wind speed (WS), and 10-meter wind direction (WD) were compared with observations (**Table S1**). The benchmarks were provided by Emery et al. (2017). For T2, despite the gross error (GE)



being slightly higher than the benchmark (≤ 2), the mean bias (MB) values ranging from -0.2 to 0.0 K fully met the benchmark (≤ 0.5). WS was slightly overestimated, indicated by positive MB values of 0.6 to 0.8 m s^{-1} , while the GE (1.4 to 1.6) and root mean square error (RMSE, 1.8 to 2.1) well met the benchmarks (≤ 2.0). Additionally, CMAQ simulations were compared with hourly observations from China National Environmental Monitoring Centre (CNMEC). Table S2 showed the model performance statistics of O_3 -1h, $\text{PM}_{2.5}$, and NO_2 . Simulated O_3 and $\text{PM}_{2.5}$ concentrations fell within the recommended standards. Specifically, although O_3 -1h was slightly overestimated, its mean normalized bias (MNB) values ranged from 0.08 to 0.15 and successfully met the $\leq \pm 0.15$ benchmark. Similarly, while $\text{PM}_{2.5}$ was underestimated, the corresponding MFB values ranged from -0.17 to 0.06, fully satisfying the $\leq \pm 0.6$ benchmark. Overall, the WRF and CMAQ model performance in this study was acceptable and comparable with previous studies, giving robust results for the subsequent process attribution analysis (Ji et al., 2024; Lyu et al., 2023).

3.2 Heatwave Increased Biogenic Emissions and O_3 Pollution

The temperature in China was higher in the summer of 2022 than in 2021 based on observations (Figs. 1b and c), with an overall increase of $\sim 1^\circ\text{C}$. In particular, the warming was most pronounced in the YRB, with the CY region experiencing an increase of over 4°C in August. In contrast, the temperatures slightly decreased in the PRD region, consistent with previous studies (Yuan et al., 2023). Model simulations also reproduced the observed high-temperature pattern in summer 2022 (Fig. S1). Besides, these elevated temperatures were accompanied by an increase in planetary boundary layer (PBL) (~ 300 m) and reductions in RH (-15%) and soil moisture (SM) (-10%), comparable with previous studies (Ding et al., 2021; García-García et al., 2023).

145

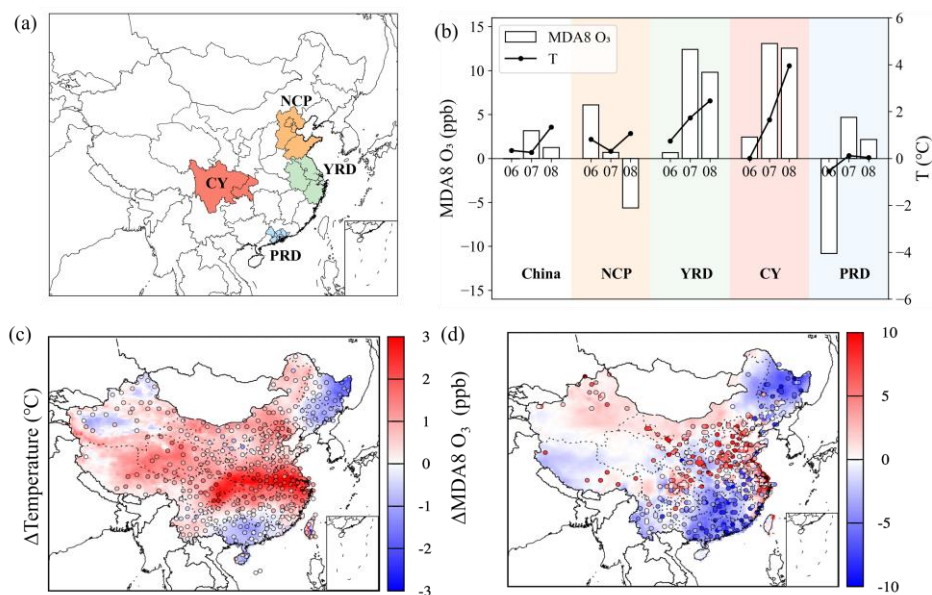


Figure 1. The observed and simulated differences in temperature and MDA8 O₃ between summer 2022 and 2021. (a) Major urban clusters in China. (b) Observed differences in temperature (T) and MDA8 O₃ between summer 2022 and 2021 (2022–2021). (c) Simulated and observed temperature differences between summer 2022 and 2021 (BASE22–BASE21, dots: observed difference). (d) Same as (c), but for MDA8 O₃.

Correspondingly, the observed MDA8 O₃ concentration in summer 2022 was higher than that in 2021 (**Fig. 1d**). The most notable increase of O₃ was also found in the YRD and CY regions, with an increase of more than 10 ppb in July and August, aligned with the greatest warming (**Figs. 1b and d**), indicating that the occurrence of secondary pollution such as O₃ was closely linked to high temperatures (Chen et al., 2024). Along with the high temperatures, simulated biogenic emission rates also increased during summer 2022 (**Fig. 2**). Notably, BVOC and SNO emissions increased in the YRD and CY regions, coinciding with the areas of most pronounced warming. In July, the BVOC emission rate in the YRD increased by 3 mole s⁻¹, whereas the SNO emission rate in NCP saw the most significant increase of over 1 μmole s⁻¹ in June. To understand how high temperatures affect secondary pollution, the following analysis separated their influence into direct meteorological effects and indirect effects mediated by biogenic emissions.

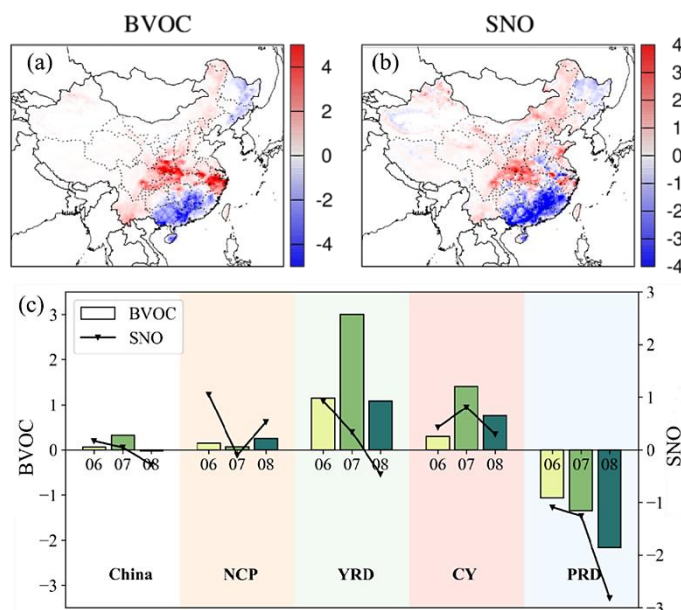


Figure 2. (a) The differences in simulated BVOC emission rates between BASE22 and BASE21 (BASE22–BASE21, units: mole s⁻¹). (b) Same as (a) but for SNO (units: μmole s⁻¹). (c) Differences of BVOC and SNO emission rates between summer 2022 and 2021 across different regions based on the MEGAN model.

3.3 Dominant Role of High-Temperature Meteorology in Secondary Pollutants

Model results showed that the MET22 case (direct meteorological impacts of high temperatures) contributed the most to secondary pollution increases (**Figs. 3a and b**). For O₃, the MET22 case accounted for over 80% of the total increase and exhibited a spatial pattern consistent with the BASE2022 case. The most pronounced increases were concentrated in the YRD and CY regions. For SOA, the BVOC22 case also made a substantial contribution, particularly in the CY region. In contrast, the SNO22 case contributed the least to secondary pollutant formation (mostly <3% for SOA) and even caused a slight SOA reduction in the CY region.

IPR analysis of the total difference between summers 2022 and 2021 identified enhanced chemical production (CHEM) and horizontal transport (HTRA) were the primary processes responsible for the O₃ rise (**Fig. S2**). Over the YRD and CY regions, where O₃ increased markedly, both CHEM and HTRA increased by more than 1.0 ppb h⁻¹ in 2022. Furthermore, more than 75% of the increases in these two processes were attributed to the MET22 case. High-temperature conditions were typically accompanied by intensified solar radiation, which accelerated chemical reaction rates and further the CHEM process (Tian et al., 2024). Such conditions were often associated with persistent high-pressure systems that favor stable and intensified synoptic-scale flows, subsequently promoting O₃ advection and its net influx into downwind areas (Tian et al., 2024).



180 3.4 Diurnal Patterns in Secondary Pollutants Driven by Atmospheric Oxidation Capacity

Diurnal variations of secondary pollutants (O_3 and SOA) across regions exhibiting significant increases (NCP, YRD, and CY) were also examined (Figs. 4 and S3). In general, the MET22 case contributed significantly to secondary pollutants during both daytime and nighttime compared to other cases. Notably, its contribution to O_3 varied regionally. The MET22 simulation showed a clear daytime contribution in the YRD and CY, whereas its contribution in the NCP was more pronounced at night.

185 For SOA, the MET22 contribution was nearly equal between day and night across these regions.

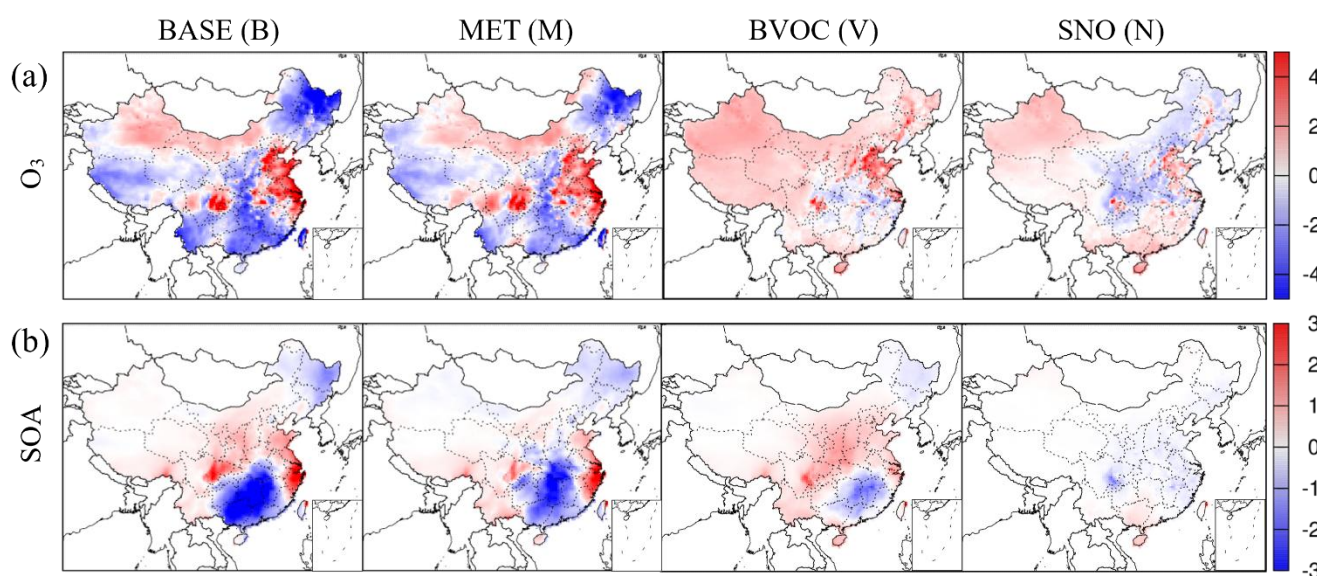
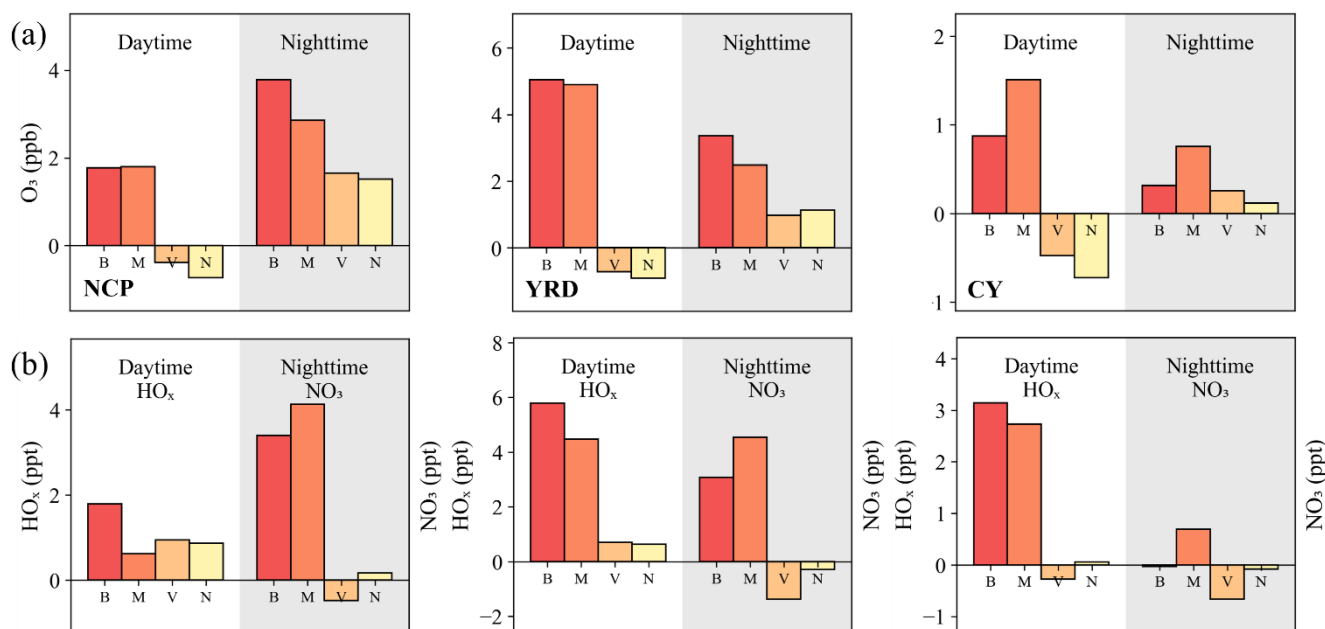


Figure 3. (a) Simulated differences in O_3 concentrations for BASE22–BASE21 (labeled ‘B’), BASE22–MET22 (labeled ‘M’), BASE22–BVOC22 (labeled ‘V’) and BASE22–SNO22 (labeled ‘N’). These scenarios represent the total differences between 2021 and 2022 (B), the contribution of meteorology (M), weather-driven BVOC (V) and SNO (N) emission changes, respectively (Units: ppb). (b) Same as (a) but for SOA (units: $\mu\text{g m}^{-3}$).

To understand this regional divergence in the diurnal MET22 response, the atmospheric oxidation capacity (AOC) was also discussed. In this study, daytime AOC is indicated by hydrogen oxide radical ($\text{HO}_x = \text{OH} + \text{HO}_2$) concentrations, while nighttime AOC was indicated by nitrate radical (NO_3) concentrations (Sillman, 1995; Zhu et al., 2021; Zhu et al., 2023; Liu et al., 2012). In general, the AOC enhancement driven by the MET22 case accounted for over 90% of the total increase in AOC, which was closely linked to the formation of secondary pollutants (Figs. 4) (Coates et al., 2016; Xing et al., 2017). For O_3 , the daytime increase in the MET22 was primarily driven by enhanced HO_x concentrations, which showed net increases of 4.5 ppt and 2.7 ppt in the YRD and CY regions, respectively (Liu et al., 2022). While daytime chemistry dominated under high-temperature conditions, concurrent high-pressure system promoted stable atmospheric conditions at night (Nasong et al., 2025). This stability led to nocturnal surface cooling, which facilitated the formation of a temperature inversion layer. This inversion inhibited the vertical diffusion of O_3 , resulting in its accumulation at ground level and a subsequent increase in NO_3



concentration. This mechanism explained the larger contribution of the MET22 case to nocturnal O₃ elevation. For SOA, both daytime formation via thermally enhanced emissions and OH oxidation and nighttime formation through NO₃/O₃ oxidation were promoted under high temperatures. Consequently, SOA contribution from the MET22 remained similar throughout the diurnal cycle.



205

Figure 4. Diurnal differences in hourly (a) O₃, (b) daytime HO_x, and nighttime NO₃ concentrations in the NCP, YRD, and CY regions, respectively. Daytime is defined as 8:00 to 20:00 and nighttime as 20:00 to 8:00 (Zhu et al., 2020; Wang et al., 2022). The differences shown are BASE22–BASE21 (labelled ‘B’) for the total change between 2021 and 2022, BASE22–MET22 (labelled ‘M’) for the contribution of meteorology; BASE22–BVOC22 (labelled ‘V’) for weather-driven BVOC emission changes; and BASE22–SNO22 (labelled ‘N’) for weather-driven SNO emission changes.

210

3.5 NCP O₃ Showed Heightened Sensitivity to BVOC Emissions

In addition to the MET22 case, the BVOC22 case (weather-driven changes in BVOC emissions) also played an important role in O₃ elevation, particularly in the NCP region (28%). Although the increase in BVOC emissions was small there (+0.15 mole s⁻¹), the resulting O₃ increase was greater than in other regions (Fig. 5). This could be explained by the VOC-limited regime in the NCP, which make O₃ highly responsive to VOC emission changes (Fig. S4). The best-fit slope method quantifies this sensitivity at 4.03 ppb s mole⁻¹ in the NCP (Fig. 6), which was an 8-fold enhancement over the national mean and a 5-to-6-fold increase compared to the YRD. These findings highlight the urgent need for enhanced VOC emission regulations within the NCP. Moreover, the impact of the BVOC22 on NCP O₃ exhibits a diurnal reversal, from negative in the daytime to positive

215



220 at night (**Fig. 4**). During the day, an increase in BVOCs enhanced the oxidation of NO to NO₂, and further facilitated the
 formation of O₃. However, the concurrently increased NO from NO₂ photolysis also intensifies the O₃ loss via titration (O₃ +
 NO). When the titration process became slightly dominant, this could lead to a net negative daytime contribution to O₃.
 Conversely, at night, increased BVOCs promoted NO₃ radical chemistry, which consumed NO and thus reduced the nocturnal
 O₃ titration. This process effectively preserved residual O₃ and facilitates its accumulation, leading to a distinct positive
 225 nighttime contribution.

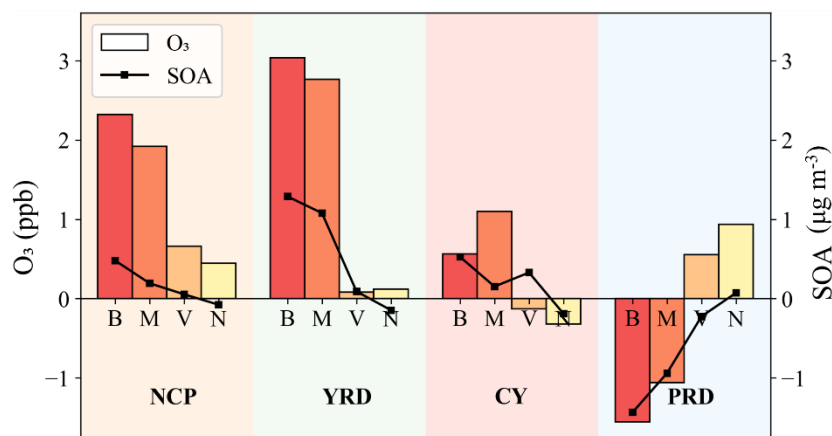


Figure 5. Changes in MDA8 O₃ and SOA are shown for BASE22–BASE21 (labelled ‘B’, total 2021–2022 change), BASE22–
 MET22 (‘M’, meteorological contribution), BASE22–BVOC22 (‘V’, weather-driven BVOC emission changes), and
 BASE22–SNO22 (‘N’, weather-driven SNO emission changes) across major urban clusters. Units are ppb and µg m⁻³ for O₃
 230 and SOA, respectively.



(a) MDA8 O ₃	China	NCP	YRD	CY	PRD
T _{max}	0.30	0.45	0.63	0.46	0.87
T	0.31	0.48	0.66	0.49	0.95
BVOCs	0.51	4.03	0.75	0.59	-0.50
SNO	0.70	2.70	1.27	0.80	0.28

(b) SOA	China	NCP	YRD	CY	PRD
T _{max}	0.14	0.11	0.28	0.28	0.08
T	0.16	0.12	0.30	0.30	0.02
BVOCs	0.53	0.74	0.46	0.50	0.09
SNO	0.51	0.49	0.63	0.58	0.10

Figure 6. Sensitivity of (a) MDA8 O₃ and (b) SOA to T_{max}, daily average temperature (T), BVOC emissions (BVOCs), and SNO emissions (SNO) across major urban clusters. MDA8 O₃ sensitivity is in ppb °C⁻¹ to temperature and ppb s mole⁻¹ to emissions. SOA sensitivity is in µg m⁻³ °C⁻¹ to temperature and µg s (m⁻³ mole⁻¹) to emissions. Values are not normalized due to differing units. Color scales are row-specific, ranging from minimum (white) to maximum (dark red).

3.6 Sensitivity Patterns of Secondary Pollutants to Temperatures and Emissions

Based on best-slope analysis, O₃ in urban areas was more sensitive to temperature changes (including both T_{max} and T) compared to the national average level (+50% to 290%, **Fig. 6**). Especially in the YRD and PRD, the sensitivity of MDA8 O₃ to temperature reached 0.66 and 0.95 ppb °C⁻¹, respectively. This was partly due to the urban heat island (UHI) effect, which elevated daytime temperatures and favored pollutant accumulation. This effect could be further intensified during heatwaves (Clinton and Gong, 2013; Delcloo et al., 2018; Wang et al., 2018).

Notably, despite a slight decrease in summer O₃ and temperature in the PRD in 2022, the region exhibited the highest O₃-temperature sensitivity, which heightened local risks and necessitated targeted mitigation. However, the correlation between O₃ and temperature was higher in the YRD than in the PRD (**Table S3**). This was because precursor emissions in the PRD were generally lower and affected by multiple factors such as sea-land breezes, which may weaken the temperature-O₃ linkage. NCP O₃ showed remarkable sensitivity to emission changes. During heatwaves, both BVOCs and SNO emissions increased. This may accelerate radical-initiated oxidation cycles and enhance OH regeneration, resulting in amplified O₃.

For SOA, the sensitivity to temperature showed pronounced regional variability, with the highest values found in the YRD and CY regions (0.28 to 0.30 µg m⁻³ °C⁻¹, **Fig. 6**), roughly twice the national average. This heightened sensitivity in the CY region is primarily driven by weather-driven biogenic emissions (the BVOC22 scenario), which contribute more significantly to SOA formation than the direct meteorological impact (MET22) (**Fig. 5**). In the extensively vegetated CY region, high temperatures markedly increase the emissions of BVOC, such as isoprene and monoterpenes (Cao et al., 2022; Guenther et al.,



255 2012). Simultaneously, the enhanced AOC during heatwaves (as discussed in **section 3.4**) rapidly oxidizes these precursors
into low-volatility products, facilitating SOA yields. Alongside BVOCs, SOA is also highly sensitive to SNO emissions in the
YRD and CY areas (0.63 and $0.58 \mu\text{g m}^{-3} \text{ }^\circ\text{C}^{-1}$, respectively, **Fig. 6**). However, the SNO22 scenario reports that reducing SNO
emissions only leads to a slight decrease in overall SOA concentrations (**Fig. 5**). Total NO_x emissions in these regions are still
dominated by anthropogenic sources (Huang et al., 2023). Although heat-induced SNO provides additional NO_x to promote
260 BVOC oxidation, fluctuations in SNO emissions have a limited impact on the total SOA concentration.
In contrast, temperature and SNO have minimal influence on SOA in the PRD. The limited contribution of heat induced SNO
is largely constrained by low precursor emissions resulting from strict regional controls (Ou et al., 2016). Furthermore, elevated
temperatures increase the saturation vapor pressure of semi-volatile organic compounds, driving their thermodynamic
partitioning back into the gas phase and thereby suppressing SOA yields (Donahue et al., 2006). In the NCP, SOA is highly
265 sensitive to BVOC emissions. Driven by high NO_x emissions and AOC alongside lower overall vegetation coverage, additional
biogenic precursors in the NCP are rapidly oxidized into SOA, leading to this pronounced sensitivity.

4 Conclusions

The 2022 summer heatwave clearly demonstrates that high temperatures drive secondary pollution through multiple pathways.
This study separates the direct meteorological effects from the indirect effects mediated by biogenic emissions. Results show
270 that direct meteorological conditions account for over 80% of the O_3 increase, particularly in the YRD and CY regions. This
dominance reflects two linked processes. First, process analysis identifies enhanced chemical production as a primary factor,
consistent with temperature-accelerated reaction kinetics. Second, horizontal transport also increased by more than 1.0 ppb h^{-1}
in these regions, indicating that the persistent high-pressure systems accompanying heatwaves not only stagnate local air but
also facilitate synoptic-scale transport of O_3 to downwind areas. Together, these mechanisms explain why the spatial pattern
275 of O_3 increase closely matches the pattern of greatest warming.

Diurnal responses reveal additional complexity. In the YRD and CY, the direct meteorological contribution to O_3 is largest
during the daytime, driven by elevated HO_x radicals. In the NCP, however, the contribution is more pronounced at night. This
regional difference arises from nocturnal surface cooling under stable high-pressure conditions, which forms a temperature
inversion that traps O_3 near the ground. The trapped O_3 then reacts with increased NO_3 radicals, creating a distinct nighttime
280 accumulation pathway. For SOA, the direct meteorological contribution is nearly equal between day and night across all
regions, suggesting that both daytime OH oxidation and nighttime NO_3/O_3 oxidation are promoted under high temperatures.
These patterns imply that heatwaves intensify atmospheric processing throughout the diurnal cycle, not only during peak
photochemical hours.

Indirect effects driven by BVOCs, while smaller overall, are critically important in specific regions. In the NCP, a modest
285 increase in BVOC emissions (0.15 mole s^{-1}) produces an O_3 response eight times the national average. This heightened
sensitivity is explained by the VOC-limited chemical regime of the NCP, where O_3 formation is highly responsive to VOC



changes. The BVOC effect also exhibits a diurnal reversal: negative during the day and positive at night. Daytime BVOC increases enhance NO-to-NO₂ conversion and O₃ formation, but the concurrent increase in NO from NO₂ photolysis also strengthens O₃ loss via titration. When titration slightly dominates, the net daytime contribution becomes negative. At night, increased BVOCs promote NO₃ chemistry, which consumes NO and reduces nocturnal O₃ titration, allowing residual O₃ to accumulate. This mechanism highlights that BVOC impacts are not simply additive but interact with background chemistry in ways that vary across the diurnal cycle.

Regional sensitivity analysis provides a quantitative basis for differentiated control strategies. O₃ in urban areas is 50-290% more sensitive to temperature than the national average, partly due to urban heat island effects. The YRD and CY show the highest SOA sensitivity to both temperature and soil NO_x emissions, indicating that coordinated precursor reductions are needed in these regions. In the PRD, O₃ shows the highest temperature sensitivity despite lower emissions, suggesting that mitigating the urban heat island itself may be necessary. In the NCP, the extreme O₃ sensitivity to BVOC emissions points to an urgent need for aggressive VOC controls. These region-specific sensitivities, derived directly from the model simulations, offer a practical framework for designing climate-informed air quality policies.

300

305

310

315



Data availability

Ground-level observation data for the key pollutants are from China's Ministry of Ecology and Environment (<https://quotsoft.net/air>). The FNL reanalysis data are from NCAR (<https://rda.ucar.edu/datasets/d083002/>). The WRF model
320 is downloaded from NCAR (<https://www.mmm.ucar.edu/models/wrf>).

Author contributions

P.W. wrote the main manuscript text, reviewed the original draft, and contributed to conceptualization and methodology. W.Y. contributed to software and validation. Z.Z. contributed to data analysis. J.L. and S.L. contributed to the visualization. H.Z. reviewed and edited the manuscript.

325 **Competing interests**

The authors declare there are no conflicts of interest for this manuscript.

Acknowledgements

The authors gratefully acknowledge the provision of ground-level pollutant data from China's Ministry of Ecology and Environment, and the FNL reanalysis data and WRF model from NCAR.

330 **Financial support**

This research was jointly funded by the National Natural Science Foundation of China (42375178) and the Natural Science Foundation of Shanghai (23ZR1406100).



References

- 335 An, N., Chen, Y., Zhai, P., Li, J., and Wei, Y.: Compound hot and ozone extremes in urban China, *Urban Climate*, 52, 101689, <https://doi.org/10.1016/j.uclim.2023.101689>, 2023.
An, Z., Huang, R. J., Zhang, R., Tie, X., Li, G., Cao, J., Zhou, W., Shi, Z., Han, Y., Gu, Z., and Ji, Y.: Severe haze in northern China: A synergy of anthropogenic emissions and atmospheric processes, *Proceedings of the National Academy of Sciences of the United States of America*, 116, 8657-8666, 10.1073/pnas.1900125116, 2019.
- 340 Bai, Y., Zhao, T., Hu, W., Zhou, Y., Xiong, J., Wang, Y., Liu, L., Shen, L., Kong, S., Meng, K., and Zheng, H.: Meteorological mechanism of regional PM_{2.5} transport building a receptor region for heavy air pollution over Central China, *Science of The Total Environment*, 808, 151951, <https://doi.org/10.1016/j.scitotenv.2021.151951>, 2022.
Byun, D.: Science algorithms of the EPA Models-3 community multi-scale air quality (CMAQ) modeling system, Cao, J., Situ, S., Hao, Y., Xie, S., and Li, L.: Enhanced summertime ozone and SOA from biogenic volatile organic compound (BVOC) emissions due to vegetation biomass variability during 1981–2018 in China, *Atmos. Chem. Phys.*, 22, 2351-2364, 10.5194/acp-22-2351-2022, 2022.
- 345 Chang, K.-H., Yu, J.-Y., Chen, T.-F., and Lin, Y.-P.: Estimating Taiwan biogenic VOC emission: Leaf energy balance consideration, *Atmospheric Environment*, 43, 5092-5100, <https://doi.org/10.1016/j.atmosenv.2009.06.038>, 2009.
Chen, T., Wang, T., Xue, L., and Brasseur, G.: Heatwave exacerbates air pollution in China through intertwined climate-energy-environment interactions, *Science Bulletin*, 69, 2765-2775, <https://doi.org/10.1016/j.scib.2024.05.018>, 2024.
- 350 Clinton, N. and Gong, P.: MODIS detected surface urban heat islands and sinks: Global locations and controls, *Remote Sensing of Environment*, 134, 294-304, <https://doi.org/10.1016/j.rse.2013.03.008>, 2013.
Coates, J., Mar, K. A., Ojha, N., and Butler, T. M.: The influence of temperature on ozone production under varying NO_x conditions – a modelling study, *Atmos. Chem. Phys.*, 16, 11601-11615, 10.5194/acp-16-11601-2016, 2016.
- 355 Conti, S., Meli, P., Minelli, G., Solimini, R., Toccaceli, V., Vichi, M., Beltrano, C., and Perini, L.: Epidemiologic study of mortality during the Summer 2003 heat wave in Italy, *Environmental Research*, 98, 390-399, <https://doi.org/10.1016/j.envres.2004.10.009>, 2005.
Delcloo, A., Duchêne, F., Hamdi, R., Berckmans, J., Deckmyn, A., and Termonia, P.: The impact of heat waves and urban heat island on the production of ozone concentrations under present and future climate conditions for the Belgian domain, *Air Pollution Modeling and its Application XXV* 35, 189-193,
- 360 Ding, H., Cao, L., Jiang, H., Jia, W., Chen, Y., and An, J.: Influence on the temperature estimation of the planetary boundary layer scheme with different minimum eddy diffusivity in WRF v3.9.1.1, *Geosci. Model Dev.*, 14, 6135-6153, 10.5194/gmd-14-6135-2021, 2021.
Donahue, N. M., Robinson, A. L., Stanier, C. O., and Pandis, S. N.: Coupled Partitioning, Dilution, and Chemical Aging of Semivolatile Organics, *Environmental Science & Technology*, 40, 2635-2643, 10.1021/es052297c, 2006.
- 365 Duan, J., Huang, R. J., Li, Y., Chen, Q., Zheng, Y., Chen, Y., Lin, C., Ni, H., Wang, M., Ovadnevaite, J., Ceburnis, D., Chen, C., Worsnop, D. R., Hoffmann, T., O'Dowd, C., and Cao, J.: Summertime and wintertime atmospheric processes of secondary aerosol in Beijing, *Atmos. Chem. Phys.*, 20, 3793-3807, 10.5194/acp-20-3793-2020, 2020.
Emery, C., Liu, Z., Russell, A. G., Odman, M. T., Yarwood, G., and Kumar, N.: Recommendations on statistics and benchmarks to assess photochemical model performance, *Journal of the Air & Waste Management Association*, 67, 582-598, 10.1080/10962247.2016.1265027, 2017.
- 370 Eremenko, M., Dufour, G., Foret, G., Keim, C., Orphal, J., Beekmann, M., Bergametti, G., and Flaud, J. M.: Tropospheric ozone distributions over Europe during the heat wave in July 2007 observed from infrared nadir spectra recorded by IASI, *Geophysical Research Letters*, 35, <https://doi.org/10.1029/2008GL034803>, 2008.
- 375 Filleul, L., Cassadou, S., Médina, S., Fabres, P., Lefranc, A., Eilstein, D., Le Tertre, A., Pascal, L., Chardon, B., Blanchard, M., Declercq, C., Jusot, J.-F., Prouvost, H., and Ledrans, M.: The Relation Between Temperature, Ozone, and Mortality in Nine French Cities During the Heat Wave of 2003, *Environmental health perspectives*, 114, 1344-1347, 10.1289/ehp.8328, 2006.
- 380 García-García, A., Cuesta-Valero, F. J., Miralles, D. G., Mahecha, M. D., Quaas, J., Reichstein, M., Zscheischler, J., and Peng, J.: Soil heat extremes can outpace air temperature extremes, *Nature Climate Change*, 13, 1237-1241, 10.1038/s41558-023-01812-3, 2023.



- Guenther, A. B., Jiang, X., Heald, C. L., Sakulyanontvittaya, T., Duhl, T., Emmons, L. K., and Wang, X.: The Model of Emissions of Gases and Aerosols from Nature version 2.1 (MEGAN2.1): an extended and updated framework for modeling biogenic emissions, *Geosci. Model Dev.*, 5, 1471-1492, 10.5194/gmd-5-1471-2012, 2012.
- 385 Hu, F. and Guo, Y.: Health impacts of air pollution in China, *Frontiers of Environmental Science & Engineering*, 15, 74, 10.1007/s11783-020-1367-1, 2020.
- Huang, J., Pan, X., Guo, X., and Li, G.: Health impact of China's Air Pollution Prevention and Control Action Plan: an analysis of national air quality monitoring and mortality data, *The Lancet. Planetary health*, 2, e313-e323, 10.1016/s2542-5196(18)30141-4, 2018.
- 390 Huang, L., Fang, J., Liao, J., Yarwood, G., Chen, H., Wang, Y., and Li, L.: Insights into soil NO emissions and the contribution to surface ozone formation in China, *Atmos. Chem. Phys.*, 23, 14919-14932, 10.5194/acp-23-14919-2023, 2023.
- Huang, R.-J., Zhang, Y., Bozzetti, C., Ho, K.-F., Cao, J.-J., Han, Y., Daellenbach, K. R., Slowik, J. G., Platt, S. M., Canonaco, F., Zotter, P., Wolf, R., Pieber, S. M., Bruns, E. A., Crippa, M., Ciarelli, G., Piazzalunga, A., Schwikowski, M., Abbaszade, G., Schnelle-Kreis, J., Zimmermann, R., An, Z., Szidat, S., Baltensperger, U., Haddad, I. E., and Prévôt, A. S. H.: High secondary aerosol contribution to particulate pollution during haze events in China, *Nature*, 514, 218-222, 10.1038/nature13774, 2014.
- 395 Huang, X., Ding, A., Wang, Z., Ding, K., Gao, J., Chai, F., and Fu, C.: Amplified transboundary transport of haze by aerosol-boundary layer interaction in China, *Nature Geoscience*, 13, 428-434, 10.1038/s41561-020-0583-4, 2020.
- Huang, X., Tang, G., Zhang, J., Liu, B., Liu, C., Zhang, J., Cong, L., Cheng, M., Yan, G., Gao, W., Wang, Y., and Wang, Y.: Characteristics of PM_{2.5} pollution in Beijing after the improvement of air quality, *Journal of Environmental Sciences*, 100, 1-10, <https://doi.org/10.1016/j.jes.2020.06.004>, 2021.
- 400 Ji, X., Chen, G., Chen, J., Xu, L., Lin, Z., Zhang, K., Fan, X., Li, M., Zhang, F., Wang, H., Huang, Z., and Hong, Y.: Meteorological impacts on the unexpected ozone pollution in coastal cities of China during the unprecedented hot summer of 2022, *Science of The Total Environment*, 914, 170035, <https://doi.org/10.1016/j.scitotenv.2024.170035>, 2024.
- 405 Li, D., Shindell, D., Ding, D., Lu, X., Zhang, L., and Zhang, Y.: Surface ozone impacts on major crop production in China from 2010 to 2017, *Atmos. Chem. Phys.*, 22, 2625-2638, 10.5194/acp-22-2625-2022, 2022.
- Li, K., Jacob, D. J., Shen, L., Lu, X., De Smedt, I., and Liao, H.: Increases in surface ozone pollution in China from 2013 to 2019: anthropogenic and meteorological influences, *Atmos. Chem. Phys.*, 20, 11423-11433, 10.5194/acp-20-11423-2020, 2020.
- 410 Li, M., Huang, X., Yan, D., Lai, S., Zhang, Z., Zhu, L., Lu, Y., Jiang, X., Wang, N., Wang, T., Song, Y., and Ding, A.: Coping with the concurrent heatwaves and ozone extremes in China under a warming climate, *Science Bulletin*, <https://doi.org/10.1016/j.scib.2024.05.034>, 2024.
- Lin, H., Ding, K., Huang, X., Lou, S., Xue, L., Wang, Z., Ma, Y., and Ding, A.: Impacts of Northward Typhoons on Autumn Haze Pollution Over North China Plain, *Journal of Geophysical Research: Atmospheres*, 129, e2023JD040465, <https://doi.org/10.1029/2023JD040465>, 2024.
- 415 Liu, T., Hong, Y., Li, M., Xu, L., Chen, J., Bian, Y., Yang, C., Dan, Y., Zhang, Y., Xue, L., Zhao, M., Huang, Z., and Wang, H.: Atmospheric oxidation capacity and ozone pollution mechanism in a coastal city of southeastern China: analysis of a typical photochemical episode by an observation-based model, *Atmos. Chem. Phys.*, 22, 2173-2190, 10.5194/acp-22-2173-2022, 2022.
- 420 Liu, Y. and Wang, T.: Worsening urban ozone pollution in China from 2013 to 2017 – Part 1: The complex and varying roles of meteorology, *Atmos. Chem. Phys.*, 20, 6305-6321, 10.5194/acp-20-6305-2020, 2020.
- Liu, Z., Wang, Y., Gu, D., Zhao, C., Huey, L. G., Stickel, R., Liao, J., Shao, M., Zhu, T., Zeng, L., Amoroso, A., Costabile, F., Chang, C. C., and Liu, S. C.: Summertime photochemistry during CAREBeijing-2007: RO_x budgets and O₃ formation, *Atmos. Chem. Phys.*, 12, 7737-7752, 10.5194/acp-12-7737-2012, 2012.
- 425 Lu, R., Xu, K., Chen, R., Chen, W., Li, F., and Lv, C.: Heat waves in summer 2022 and increasing concern regarding heat waves in general, *Atmospheric and Oceanic Science Letters*, 16, 100290, <https://doi.org/10.1016/j.aosl.2022.100290>, 2023.
- Luo, M. and Lau, N.-C.: Heat Waves in Southern China: Synoptic Behavior, Long-Term Change, and Urbanization Effects, *Environ Sci Technol*, 30, 703-720, <https://doi.org/10.1175/JCLI-D-16-0269.1>, 2017.
- Lyu, X., Li, K., Guo, H., Morawska, L., Zhou, B., Zeren, Y., Jiang, F., Chen, C., Goldstein, A. H., Xu, X., Wang, T., Lu, X., 430 Zhu, T., Querol, X., Chatani, S., Latif, M. T., Schuch, D., Sinha, V., Kumar, P., Mullins, B., Seguel, R., Shao, M., Xue, L.,



- Wang, N., Chen, J., Gao, J., Chai, F., Simpson, I., Sinha, B., and Blake, D. R.: A synergistic ozone-climate control to address emerging ozone pollution challenges, *One Earth*, 6, 964-977, <https://doi.org/10.1016/j.oneear.2023.07.004>, 2023.
- Ma, M., Gao, Y., Wang, Y., Zhang, S., Leung, L. R., Liu, C., Wang, S., Zhao, B., Chang, X., Su, H., Zhang, T., Sheng, L., Yao, X., and Gao, H.: Substantial ozone enhancement over the North China Plain from increased biogenic emissions due to heat waves and land cover in summer 2017, *Atmos. Chem. Phys.*, 19, 12195-12207, 10.5194/acp-19-12195-2019, 2019.
- 435 Megaritis, A. G., Fountoukis, C., Charalampidis, P. E., Pilinis, C., and Pandis, S. N.: Response of fine particulate matter concentrations to changes of emissions and temperature in Europe, *Atmos. Chem. Phys.*, 13, 3423-3443, 10.5194/acp-13-3423-2013, 2013.
- Meng, X., Jiang, J., Chen, T., Zhang, Z., Lu, B., Liu, C., Xue, L., Chen, J., Herrmann, H., and Li, X.: Chemical drivers of ozone change in extreme temperatures in eastern China, *Science of The Total Environment*, 874, 162424, <https://doi.org/10.1016/j.scitotenv.2023.162424>, 2023.
- 440 Mousavinezhad, S., Choi, Y., Pouyaei, A., Ghahremanloo, M., and Nelson, D. L.: A comprehensive investigation of surface ozone pollution in China, 2015–2019: Separating the contributions from meteorology and precursor emissions, *Atmospheric Research*, 257, 105599, <https://doi.org/10.1016/j.atmosres.2021.105599>, 2021.
- 445 Nasong, D., Zhou, S., Kornhuber, K., and Yu, B.: Concurrent Heat Extremes in Relation to Global Warming, High Atmospheric Pressure and Low Soil Moisture in the Northern Hemisphere, *Earth's Future*, 13, e2024EF005256, <https://doi.org/10.1029/2024EF005256>, 2025.
- Oh, H.-J., Chen, Y., and Kim, H.: Deposition of secondary organic aerosol in human lung model: Effect of photochemically aged aerosol on human respiratory system, *Ecotoxicology and Environmental Safety*, 265, 115497, <https://doi.org/10.1016/j.ecoenv.2023.115497>, 2023.
- 450 Oikawa, P. Y., Ge, C., Wang, J., Eberwein, J. R., Liang, L. L., Allsman, L. A., Grantz, D. A., and Jenerette, G. D.: Unusually high soil nitrogen oxide emissions influence air quality in a high-temperature agricultural region, *Nature Communications*, 6, 8753, 10.1038/ncomms9753, 2015.
- Oke, T. R.: The energetic basis of the urban heat island, *Quarterly Journal of the Royal Meteorological Society*, 108, 1-24, <https://doi.org/10.1002/qj.49710845502>, 1982.
- 455 Otero, N., Sillmann, J., Schnell, J. L., Rust, H. W., and Butler, T.: Synoptic and meteorological drivers of extreme ozone concentrations over Europe, *Environmental Research Letters*, 11, 024005, 10.1088/1748-9326/11/2/024005, 2016.
- Ou, J., Yuan, Z., Zheng, J., Huang, Z., Shao, M., Li, Z., Huang, X., Guo, H., and Louie, P. K. K.: Ambient Ozone Control in a Photochemically Active Region: Short-Term Despiking or Long-Term Attainment?, *Environmental Science & Technology*, 50, 5720-5728, 10.1021/acs.est.6b00345, 2016.
- 460 Seco, R., Holst, T., Davie-Martin, C. L., Simin, T., Guenther, A., Pirk, N., Rinne, J., and Rinnan, R.: Strong isoprene emission response to temperature in tundra vegetation, *Proceedings of the National Academy of Sciences*, 119, e2118014119, 10.1073/pnas.2118014119, 2022.
- Shao, T., Wang, P., Yu, W., Gao, Y., Zhu, S., Zhang, Y., Hu, D., Zhang, B., and Zhang, H.: Drivers of alleviated PM_{2.5} and O₃ concentrations in China from 2013 to 2020, *Resources, Conservation and Recycling*, 197, 107110, <https://doi.org/10.1016/j.resconrec.2023.107110>, 2023.
- 465 Sillman, S.: The use of NO_y, H₂O₂, and HNO₃ as indicators for ozone-NO_x-hydrocarbon sensitivity in urban locations, *Journal of Geophysical Research: Atmospheres*, 100, 14175-14188, <https://doi.org/10.1029/94JD02953>, 1995.
- Su, X., Yan, X., and Tsai, C.-L.: Linear regression, *WIREs Computational Statistics*, 4, 275-294, <https://doi.org/10.1002/wics.1198>, 2012.
- 470 Sun, Y., Zhang, X., Zwiers, F. W., Song, L., Wan, H., Hu, T., Yin, H., and Ren, G.: Rapid increase in the risk of extreme summer heat in Eastern China, *Nature Climate Change*, 4, 1082-1085, 10.1038/nclimate2410, 2014.
- Tian, Y., Kleidon, A., Lesk, C., Zhou, S., Luo, X., Ghausi, S. A., Wang, G., Zhong, D., and Zscheischler, J.: Characterizing heatwaves based on land surface energy budget, *Communications Earth & Environment*, 5, 617, 10.1038/s43247-024-01784-y, 2024.
- 475 Wang, H., Wu, K., Liu, Y., Sheng, B., Lu, X., He, Y., Xie, J., Wang, H., and Fan, S.: Role of Heat Wave-Induced Biogenic VOC Enhancements in Persistent Ozone Episodes Formation in Pearl River Delta, *Journal of Geophysical Research: Atmospheres*, 126, e2020JD034317, <https://doi.org/10.1029/2020JD034317>, 2021a.



- 480 Wang, J., Wang, D., Ge, B., Lin, W., Ji, D., Pan, X., Li, J., and Wang, Z.: Increase in daytime ozone exposure due to nighttime accumulation in a typical city in eastern China during 2014–2020, *Atmospheric Pollution Research*, 13, 101387, <https://doi.org/10.1016/j.apr.2022.101387>, 2022.
- 485 Wang, J., Ye, J., Zhang, Q., Zhao, J., Wu, Y., Li, J., Liu, D., Li, W., Zhang, Y., Wu, C., Xie, C., Qin, Y., Lei, Y., Huang, X., Guo, J., Liu, P., Fu, P., Li, Y., Lee, H. C., Choi, H., Zhang, J., Liao, H., Chen, M., Sun, Y., Ge, X., Martin, S. T., and Jacob, D. J.: Aqueous production of secondary organic aerosol from fossil-fuel emissions in winter Beijing haze, *Proceedings of the National Academy of Sciences*, 118, e2022179118, 10.1073/pnas.2022179118, 2021b.
- 490 Wang, N., Lyu, X., Deng, X., Huang, X., Jiang, F., and Ding, A.: Aggravating O₃ pollution due to NO_x emission control in eastern China, *Science of The Total Environment*, 677, 732–744, <https://doi.org/10.1016/j.scitotenv.2019.04.388>, 2019.
- 490 Wang, N., Du, Y., Chen, D., Meng, H., Chen, X., Zhou, L., Shi, G., Zhan, Y., Feng, M., Li, W., Chen, M., Li, Z., and Yang, F.: Spatial disparities of ozone pollution in the Sichuan Basin spurred by extreme, hot weather, *Atmos. Chem. Phys.*, 24, 3029–3042, 10.5194/acp-24-3029-2024, 2024.
- Wang, Y., Du, H., Xu, Y., Lu, D., Wang, X., and Guo, Z.: Temporal and spatial variation relationship and influence factors on surface urban heat island and ozone pollution in the Yangtze River Delta, China, *Science of The Total Environment*, 631–632, 921–933, <https://doi.org/10.1016/j.scitotenv.2018.03.050>, 2018.
- 495 Weng, Z., Tong, D., Wu, S., and Xie, Y.: Improved air quality from China’s clean air actions alleviates health expenditure inequality, *Environment International*, 173, 107831, <https://doi.org/10.1016/j.envint.2023.107831>, 2023.
- Xing, J., Wang, J., Mathur, R., Wang, S., Sarwar, G., Pleim, J., Hogrefe, C., Zhang, Y., Jiang, J., Wong, D. C., and Hao, J.: Impacts of aerosol direct effects on tropospheric ozone through changes in atmospheric dynamics and photolysis rates, *Atmos. Chem. Phys.*, 17, 9869–9883, 10.5194/acp-17-9869-2017, 2017.
- 500 Yuan, Y., Liao, Z., Zhou, B., and Zhai, P.: Unprecedented Hot Extremes Observed in City Clusters in China during Summer 2022, *Journal of Meteorological Research*, 37, 141–148, 10.1007/s13351-023-2184-9, 2023.
- 505 Zhang, H., Yee, L. D., Lee, B. H., Curtis, M. P., Worton, D. R., Isaacman-VanWertz, G., Offenberg, J. H., Lewandowski, M., Kleindienst, T. E., Beaver, M. R., Holder, A. L., Lonneman, W. A., Docherty, K. S., Jaoui, M., Pye, H. O. T., Hu, W., Day, D. A., Campuzano-Jost, P., Jimenez, J. L., Guo, H., Weber, R. J., de Gouw, J., Koss, A. R., Edgerton, E. S., Brune, W., Mohr, C., Lopez-Hilfiker, F. D., Lutz, A., Kreisberg, N. M., Spielman, S. R., Hering, S. V., Wilson, K. R., Thornton, J. A., and Goldstein, A. H.: Monoterpenes are the largest source of summertime organic aerosol in the southeastern United States, *Proceedings of the National Academy of Sciences*, 115, 2038–2043, 10.1073/pnas.1717513115, 2018.
- Zhang, J., Su, Y., Chen, C., Guo, W., Tan, Q., Feng, M., Song, D., Jiang, T., Chen, Q., Li, Y., Li, W., Wang, Y., Huang, X., Han, L., Wu, W., and Wang, G.: Chemical composition, sources and formation mechanism of urban PM_{2.5} in Southwest China: a case study at the beginning of 2023, *Atmos. Chem. Phys.*, 24, 2803–2820, 10.5194/acp-24-2803-2024, 2024.
- 510 Zhang, Q., Zheng, Y., Tong, D., Shao, M., Wang, S., Zhang, Y., Xu, X., Wang, J., He, H., Liu, W., Ding, Y., Lei, Y., Li, J., Wang, Z., Zhang, X., Wang, Y., Cheng, J., Liu, Y., Shi, Q., Yan, L., Geng, G., Hong, C., Li, M., Liu, F., Zheng, B., Cao, J., Ding, A., Gao, J., Fu, Q., Huo, J., Liu, B., Liu, Z., Yang, F., He, K., and Hao, J.: Drivers of improved PM_{2.5} air quality in China from 2013 to 2017, *Proceedings of the National Academy of Sciences*, 116, 24463–24469, 10.1073/pnas.1907956116, 2019.
- 515 Zhang, Y., Dai, J., Li, Q., Chen, T., Mu, J., Brasseur, G., Wang, T., and Xue, L.: Biogenic volatile organic compounds enhance ozone production and complicate control efforts: Insights from long-term observations in Hong Kong, *Atmospheric Environment*, 309, 119917, <https://doi.org/10.1016/j.atmosenv.2023.119917>, 2023.
- Zhao, B., Zheng, H., Wang, S., Smith, K. R., Lu, X., Aunan, K., Gu, Y., Wang, Y., Ding, D., Xing, J., Fu, X., Yang, X., Liou, K.-N., and Hao, J.: Change in household fuels dominates the decrease in PM_{2.5} exposure and premature mortality in China in 2005–2015, *Proceedings of the National Academy of Sciences*, 115, 12401–12406, 10.1073/pnas.1812955115, 2018.
- 520 Zheng, B., Tong, D., Li, M., Liu, F., Hong, C., Geng, G., Li, H., Li, X., Peng, L., Qi, J., Yan, L., Zhang, Y., Zhao, H., Zheng, Y., He, K., and Zhang, Q.: Trends in China’s anthropogenic emissions since 2010 as the consequence of clean air actions, *Atmos. Chem. Phys.*, 18, 14095–14111, 10.5194/acp-18-14095-2018, 2018.
- 525 Zheng, Y., Xue, T., Zhang, Q., Geng, G.-n., Tong, D., Li, X., and He, K. J. E. R. L.: Air quality improvements and health benefits from China’s clean air action since 2013, 12, 2017.
- Zhu, S., Ma, J., Wang, S., Sun, S., Wang, P., and Zhang, H.: Shifts of Formation Regimes and Increases of Atmospheric Oxidation Led to Ozone Increase in North China Plain and Yangtze River Delta From 2016 to 2019, *Journal of Geophysical Research: Atmospheres*, 128, e2022JD038373, <https://doi.org/10.1029/2022JD038373>, 2023.



530 Zhu, S., Poetzscher, J., Shen, J., Wang, S., Wang, P., and Zhang, H.: Comprehensive Insights Into O₃ Changes During the COVID-19 From O₃ Formation Regime and Atmospheric Oxidation Capacity, *Geophysical Research Letters*, 48, e2021GL093668, <https://doi.org/10.1029/2021GL093668>, 2021.

Zhu, X., Ma, Z., Li, Z., Wu, J., Guo, H., Yin, X., Ma, X., and Qiao, L.: Impacts of meteorological conditions on nocturnal surface ozone enhancement during the summertime in Beijing, *Atmospheric Environment*, 225, 117368, <https://doi.org/10.1016/j.atmosenv.2020.117368>, 2020.

535